Heavy residue excitation functions for the collisions 6, 7Li + 64Zn near the Coulomb barrier

Di Pietro, A.; Figuera, P.; Strano, E.; Fisichella, M.; Goryunov, O.; Lattuada, M.; Maiolino, C.; Marchetta, C.; Milin, Matko; Musumarra, A.; ...

Heavy residue excitation functions for the collisions ^{6,7}Li + ^{64}Zn near the Coulomb barrier

A. Di Pietro,[1] P. Figuera,[1] E. Strano,[1,2,*] M. Fisichella,[1,3,4] O. Goryunov,[5] M. Lattuada,[1,2] C. Maiolino,[1] C. Marchetta,[1] M. Milin,[6] A. Musumarra,[1,2] V. Ostashko,[5] M. G. Pellegriti,[1,2] V. Privitera,[7] G. Randisi,[1,2] L. Romano,[2,7] D. Santonocito,[1] V. Scuderi,[1,2] D. Torresi,[1,4,*] and M. Zadro[8]

[1]*INFN-Laboratori Nazionali del Sud, Catania, Italy*
[2]*Dipartimento di Fisica ed Astronomia Universitá di Catania, Catania, Italy*
[3]*Dipartimento di Fisica Universitá di Messina, Messina, Italy*
[4]*Centro Siciliano di Fisica Nucleare e Struttura della Materia, Catania, Italy*
[5]*KINR, Kiev, Ukraine*
[6]*Department of Physics Faculty of Science University of Zagreb, Zagreb, Croatia*
[7]*CNR-IMM MATIS, Catania, Italy*
[8]*Division of Experimental Physics Ruđer Bošković Institute, Zagreb, Croatia*

(Received 25 February 2013; revised manuscript received 13 May 2013; published 27 June 2013)

Excitation functions for the production of heavy residues have been measured for the collisions ^{6,7}Li + ^{64}Zn at energies around and below the Coulomb barrier. The cross sections for heavy residue production have been measured using an activation technique, detecting off-line the characteristic atomic x-rays emitted in the electron capture decay of the reaction products. The experimental relative yields of the residues have been compared with statistical model calculations performed by using the code CASCADE. Such a comparison suggests that heavy residue production is dominated by complete fusion at above-barrier energies, whereas different processes like incomplete fusion and/or transfer become dominant in the sub-barrier energy region. The heavy residue excitation function ratio between the ^{6}Li- and ^{7}Li-induced collisions shows an increasing trend as the energy decreases below the barrier.

DOI: 10.1103/PhysRevC.87.064614 PACS number(s): 25.70.Jj, 25.70.Gh

I. INTRODUCTION

The study of nuclear collisions involving halo or, more in general, weakly bound nuclei at energies around the Coulomb barrier had considerable interest in the last decade. In fact, the peculiar structure of such nuclei, which have very low breakup thresholds and an extended matter distribution, can strongly influence the reaction mechanisms around the Coulomb barrier (see, e.g., Refs. [1–5], and references therein). One expects that direct processes like breakup or transfer can be favored by the low breakup thresholds and by the cluster or halo structure of such nuclei. Owing to the low breakup threshold, coupling effects to the continuum are expected to have an important role on fusion and elastic scattering, and a complete description of such processes requires complex continuum-discretized coupled-channels (CDCC) calculations (see, e.g., Refs. [1,2,4,6], and references therein).

As an example, because coupling to the continuum is generating a repulsive polarization potential (see, e.g., Refs. [7,8]), the usual threshold anomaly in the optical potential (OP) owing to the presence of an attractive polarization potential can disappear in collisions between weakly bound nuclei. An increase of the imaginary part at the barrier with a small decrease in the real part, or a rather flat behavior of the real and imaginary parts as a function of the energy, can be observed. This new kind of dependence of the OP on the energy, characterized by the absence of the usual threshold anomaly, has been called *breakup threshold anomaly* in the literature (see, e.g., Refs. [9–14]).

The fusion cross sections may be affected by dynamical effects owing to coupling not only to bound states, but also to the continuum, and by static effects owing to the fact that the diffuse surface of these nuclei affects the shape of the projectile-target potential, thus reducing the Coulomb barrier. Moreover, owing to the large breakup probability, in addition to complete fusion (CF) one can have a non-negligible contribution of incomplete fusion (ICF). The sum of the CF and ICF cross sections is usually defined as total fusion (TF) cross section. In fusion-evaporation reactions induced by weakly bound nuclei on heavy targets (see, e.g., Refs. [15–18]), where the emission of charged particles is hindered by the presence of a strong Coulomb barrier, the CF and ICF contributions can be usually clearly separated because they produce evaporation residues (ERs) of different charge. On the contrary, for fusion of weakly bound nuclei on medium mass or light targets (see, e.g., Refs. [19–24]), the same residue can be populated by the CF and ICF mechanisms, making their separation much more difficult. For this reason most of the fusion data for light and medium mass systems are relative to TF.

Recently, a consistent systematic comparison of many published fusion excitation functions for collisions induced by weakly bound nuclei on targets of different mass was performed in Refs. [25,26]. It was concluded that coupling to continuum or transfer has the following effects. In collisions on heavy targets, where CF and ICF can be separated, CF is suppressed above the barrier and enhanced below; at the same time TF shows no effects above the barrier and enhancement below the barrier. In collisions on medium mass or light

*Present address: INFN-Sezione di Padova, Padova, Italy.

targets, no effects on the existing TF cross sections appear to be present, although the amount of available data below the barrier is limited and new data are necessary to better infer a systematic behavior.

To give further contribution to the study of the above-mentioned topic, we measured the heavy residue production cross sections for the collisions ^{6,7}Li + ^{64}Zn at several energies around and below the Coulomb barrier. The two stable lithium isotopes have among the lowest binding energies of all stable nuclides. In particular, ^{6}Li in its ground state has an $\alpha + d$ cluster structure with a separation energy of 1.47 MeV, lower than the ^{7}Li one (2.47 MeV), which shows an $\alpha + t$ cluster structure. Moreover, the ^{6}Li nucleus has no bound excited states, whereas the ^{7}Li one has one bound excited state at $E^{*} = 478$ keV. The different structure of ^{6}Li and ^{7}Li might influence the reaction dynamics differently. An example of possible effects of these differences on the dynamics of the collision is discussed in Refs. [23,27], where the TF excitation functions for ^{6}Li and ^{7}Li on a ^{59}Co target have been measured. At sub-barrier energies, an enhancement in the TF cross section for the collision induced by ^{6}Li with respect to the corresponding one induced by ^{7}Li has been observed. The authors concluded that this behavior could be explained only taking into account the coupling with the continuum and the different binding energy of the two nuclei [27]. A similar behavior has also been observed by other authors (see, e.g., Refs. [22,24]).

Total fusion excitation functions for the ^{6,7}Li + ^{64}Zn systems have already been presented in Ref. [19], in an energy range mainly extending in the region above the Coulomb barrier. These cross sections have been extracted via the direct detection of the ERs emitted in the reaction. It was later pointed out that, in the above-mentioned systematic comparison of the fusion experimental data for several systems [25,26], the ^{6,7}Li + ^{64}Zn TF excitation functions of Ref. [19] deviate from the systematics [26]. As a consequence, the presence of a possible underestimation of the ^{6,7}Li + ^{64}Zn TF cross sections in Ref. [19] has been suggested in Ref. [26].

Our measurement of heavy residue production excitation functions for ^{6,7}Li + ^{64}Zn was performed by using an activation technique; this does not present the experimental problems associated with the direct detection of the very low energy ERs, allowing the extraction of the cross sections at energies far below the Coulomb barrier. The main aims of the present experiment were the following: to measure the cross sections in a wider energy range extending well below the barrier; to cross-check the old results of Ref. [19] with a different experimental technique; to look for possible differences in the excitation functions owing to the different structures of ^{6,7}Li, as the ones previously mentioned [22–24]. Moreover, because the used technique allows for mass and charge identification of the detected residues, another goal of the present experiment is to compare the experimental relative yield of the ERs with the prediction of statistical model calculations to get information on the competition between CF and other possible reaction mechanisms such as ICF or transfer.

This work is organized as follows. In Sec. II we describe the procedure used to extract the production cross sections for the different heavy residues. Then, in Sec. III, the obtained results are discussed and compared with the ones of other authors. Finally, the main conclusions of the present study are summarized in Sec. IV.

II. EXPERIMENTAL DETAILS

The heavy residue (HR) production cross sections for the systems ^{6,7}Li + ^{64}Zn, around and below the barrier, were measured by using an activation technique. The direct HR detection would indeed be limited by the fact that a certain fraction of them may not have enough kinetic energy to emerge from the target or may emerge with an energy which can be below the detection or identification thresholds. The technique used is based on two main steps. The first step consists in the irradiation of a ^{64}Zn target, followed by a catcher of a different material, which stops all the HR produced in the collisions. The second step consists of the off-line detection of the atomic x-rays, emitted after the electron capture decay of the residues. As we discuss in the following, the analysis of the x-ray spectra and associated decay curves makes it possible to reconstruct the production cross sections of the different HR identified in mass and charge. This technique is suitable for the studied systems. In fact, according to statistical model calculations, most of the HR production cross section associated with CF or ICF reactions is attributable to nuclides which decay by electron capture, with half-lives approximately in the range between 15 min and 1 yr. The same technique has already been successfully applied by our group to measure the fusion excitation functions of the systems ^{4,6}He + ^{64}Zn [28–30].

In the next sections we describe the experimental procedures associated with the activation of the Zn targets, the subsequent off-line x-ray detection, and the reconstruction of the production cross sections.

A. Activation measurements

The experiments have been performed at the SMP Tandem of the Laboratori Nazionali del Sud in Catania. The experimental setup used in the activation measurements was mounted inside a scattering chamber having a diameter of 2 m and is sketched in Fig. 1.

For each bombarding energy the Li beam first crossed a thin (70 μg/cm^2) Au foil and then impinged on a ^{64}Zn target

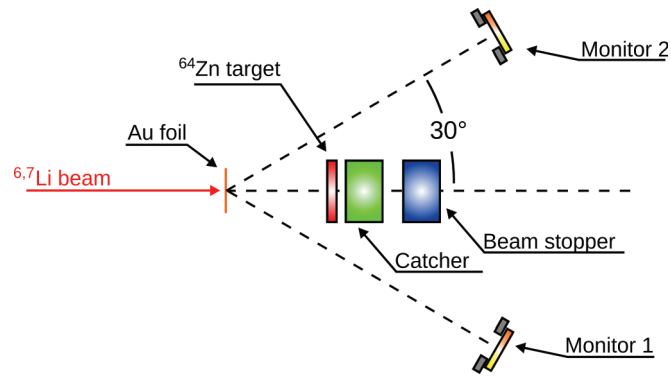

FIG. 1. (Color online) Sketch of the experimental setup used for the activation of the targets. See text for details.

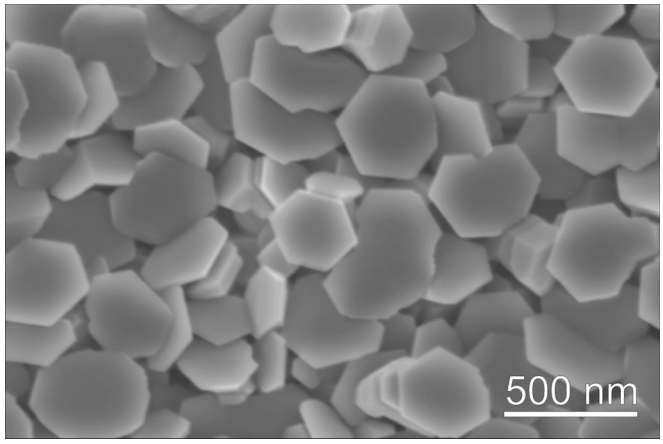

FIG. 2. SEM plan view of the ^{64}Zn target surface.

evaporated onto a catcher. The typical average thickness of the ^{64}Zn targets was around 250 μg/cm^2 (0.35 μm) with a corresponding beam energy loss inside the targets of around 150–200 keV in the explored bombarding energy range. Catcher foils were made of ^{93}Nb 2.5 mg/cm^2 thick at above barrier energies. In the activation runs at sub-barrier energies we used ^{165}Ho catcher foils 3.0 mg/cm^2 thick, because they generated a lower continuum background in the energy region of interest around 10 keV. Information on thickness and uniformity of the used Zn targets and associated catchers has been deduced measuring energy loss spectra of α particles emitted by an ^{241}Am source crossing the foils. Owing to target nonuniformity, the experimental spectrum is larger than the one calculated by SRIM [31] and, from the comparison, a Zn target thickness distribution with a full width at half maximum of about 0.150 μm has been deduced. The surface morphology of the targets was investigated by scanning electron microscopy (SEM) in plan view by a field emission Zeiss Supra 25 microscope. Figure 2 shows that the target surface is characterized by the presence of hexagonal crystals whose typical size and orientation appears to be consistent with the Zn layer nonuniformity estimated from the energy loss spectrum.

The Li beams have been collimated by the combination of a 4 × 4 mm^2 square collimator, placed 156 cm upstream from the Au foil, and a 3.5-mm-diameter circular collimator, placed 5 cm upstream from the Au foil. An additional antiscattering collimator was placed 2 cm upstream from the Au foil. In the reaction chamber the stack holder has been mounted on a rotating plate to allow its removal during the beam focusing procedures. The alignment and beam collimation procedures were cross checked by irradiating a radiation-sensitive foil placed at the target position, before and after the end of the experiment. As we discuss in the next sections, to properly reconstruct the production cross sections, it is necessary to know the beam current as a function of time during the irradiation. To this aim, two monitor detectors were placed symmetrically on both sides of the beam to detect the beam particles diffused by the Au foil by pure Rutherford scattering, and a pulser at known fixed frequency was read by the acquisition. Each Si monitor detector was placed at 30° with respect to the beam direction at a distance of 87 cm from the Au foil and had a circular collimator with a diameter

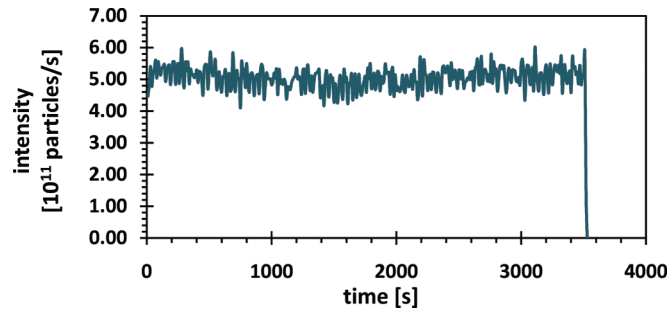

FIG. 3. (Color online) Beam current as function of time reconstructed for the activation performed using ^{6}Li at 20 MeV.

of 4.0 mm. The beam current as a function of time was then reconstructed off-line taking into account the Au target thickness, the Rutherford cross section, the pulser frequency, and the monitors' solid angle. As an example, in Fig. 3 we show the reconstructed current-versus-time curve for the ^{6}Li irradiation performed at 20 MeV.

B. Analysis of the x-ray spectra and activity curves

The delayed x-ray activity, following the electron capture decay of the residues, was measured off-line, using lead-shielded ORTEC lithium-drifted silicon detectors Si(Li). Such detectors had a diameter of 16 mm, an active thickness of 5 mm, and a Be entrance window 50 μm thick. Their intrinsic efficiency is 100% for the x-ray energies of interest (around 10 keV). Immediately after the end of each activation run, the ^{64}Zn foil and its associated catcher were taken from the reaction chamber and were moved to the laboratory for the activity measurement, where they were placed in front of a Si(Li) detector. The Zn foil and associated catcher were placed in a plastic holder to fix their position with respect to the detector, hence reducing the error on the efficiency owing to uncertainties in the geometry. The distance between the foils and the crystal was ≈10 mm. The detector end cup with the foil and associated holder were surrounded by a cylindrical lead shield 5 cm thick. Two identical setups were used to follow the decay of the foils for a period of about 6 months after the end of the activation.

The absolute x-ray detection efficiency, as well as its indetermination associated with uncertainties in the target-detector distance and beam spot position and diameter were calculated performing Monte Carlo simulations. We obtained a calculated efficiency of (7.3 ± 0.7)%, where the indetermination is essentially attributable to the estimated uncertainty on the target-detector distance. The absolute efficiency value obtained via the Monte Carlo calculations was cross-checked experimentally by using a ^{55}Fe source, whose activity was certified within ±3.5%. An efficiency value in agreement with the Monte Carlo calculations, within the indetermination of the source activity, was obtained.

The energy calibration of the detectors was performed by using a ^{109}Cd source and the x-ray fluorescence induced on Zr, Cu, and Fe.

Typical measured x-ray energy spectra are shown in Fig. 4. Spectra in Figs. 4(a)–4(c) concern the collision

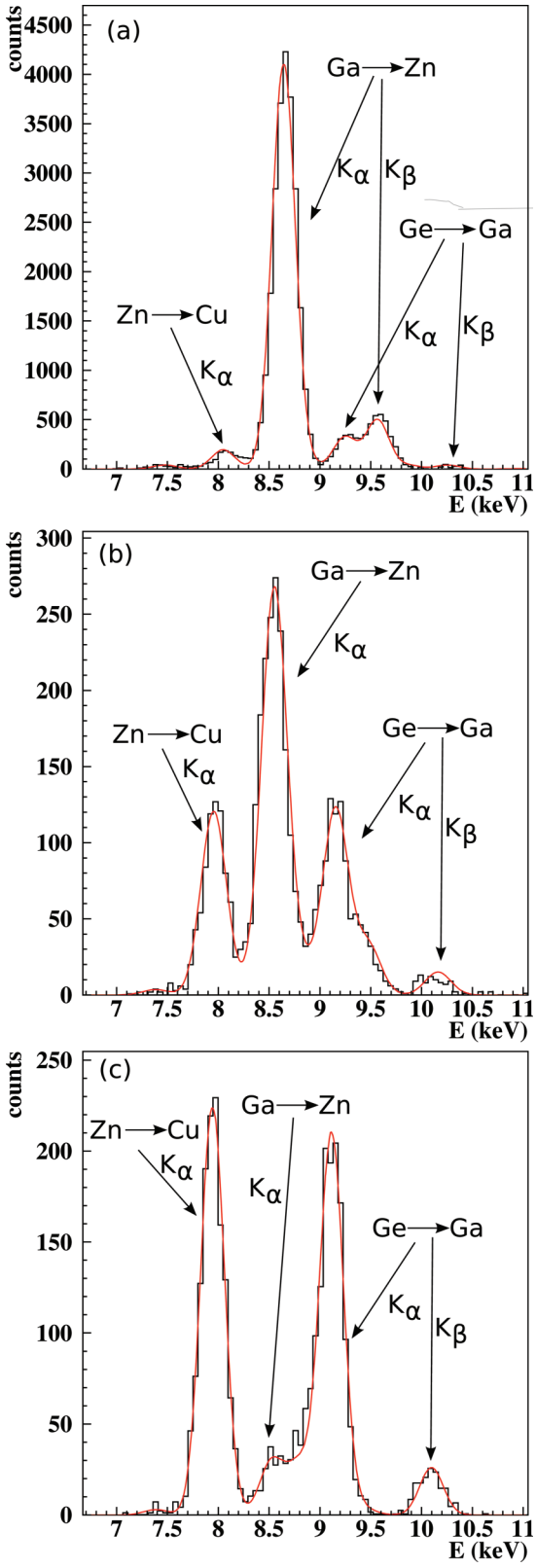

FIG. 4. (Color online) Off-line x-ray energy spectra for the collision ^{6}Li + ^{64}Zn at 20 MeV measured: (a) 7 h after the end of the activation; (b) 12 d after the end of the activation; (c) 82 d after the end of the activation.

^{6}Li + ^{64}Zn at 20 MeV and were measured 7 h, 12 d, and 82 d after the end of the activation, respectively. As one can see, just after the end of the activation, the spectra are dominated by the yield of the short-lived Ga isotopes, although the lines of the long-lived Ge and Zn isotopes are also visible. On the contrary, the yields of the long-lived Ge and Zn isotopes become dominant after some weeks. The peak integration has been performed by fitting each spectrum as the sum of several overlapped Gaussian functions. To reduce the number of free parameters, the known ratio between the yields associated to the K_α and K_β lines (see, e.g., Ref. [32]) has been imposed as ratio between the areas of the two corresponding Gaussian functions. In addition, supposing that the peak width is mostly correlated to the detector energy resolution, this parameter has been assumed to be the same for all the peaks. Because the energy calibration is known, the position of the K_α and K_β lines in the fit has been fixed as well. Therefore, the only free parameters in the fit were the integrals of all K_α peaks and their width which was the same for all peaks. The continuous lines in Fig. 4 show the result of the fit procedure. This fitting procedure takes into account the partial superimposition of the K_α and K_β lines related to the decay of HR having neighboring charge Z. Detection of x-rays produced in reactions between the incident beam and the used catcher foils was not a problem, because the associated characteristic x-ray energies were completely separated from the ones of interest.

As one can see in Fig. 4, the x-ray spectra are giving us information only on the charge Z of the HRs produced in the reactions. However, because different isotopes of the same element have different half-lives, their contribution can be unfolded by analyzing the activity as function of time associated with each K_α peak in the x-ray energy spectra. This method is particularly suitable in the present case, because the half-lives of all expected HRs are neither too short nor too long, ranging between 15 min to about 1 yr. The acquisition system used for the off-line x-ray measurements stored on disk the computer time for each event and, moreover, it was also triggered by a pulser at constant known frequency. This made it possible to reconstruct the activity curves taking the acquisition dead time properly into account (although it was negligible in most of the off-line runs) and, when necessary, to split long runs in more parts during the analysis.

As an example, in Figs. 5 and 6 we show the activity curves for the Ga and Ge peaks, respectively, relative to the collision ^{6}Li + ^{64}Zn at 20 MeV. The time $t = 0$ in the curves corresponds to the end of the foil activation. As expected, in the used semilogarithmic scale, one can clearly distinguish different slopes corresponding to the contribution of isotopes with different half-lives. To determine the production cross section for each isotope in the stack, it is necessary to know the activity at the end of the activation step for each of them. Such activities were determined by fitting the overall activity curve as the sum of its exponential contributions, each corresponding to a known half-life. The best fit has been carried out by χ^2 minimization. As a result of the fit procedure, one obtains the activity $A(0)$ exactly at the end of the activation step for each of the isotopes in the stack. The procedure used to convert this information into cross sections is discussed in the next section.

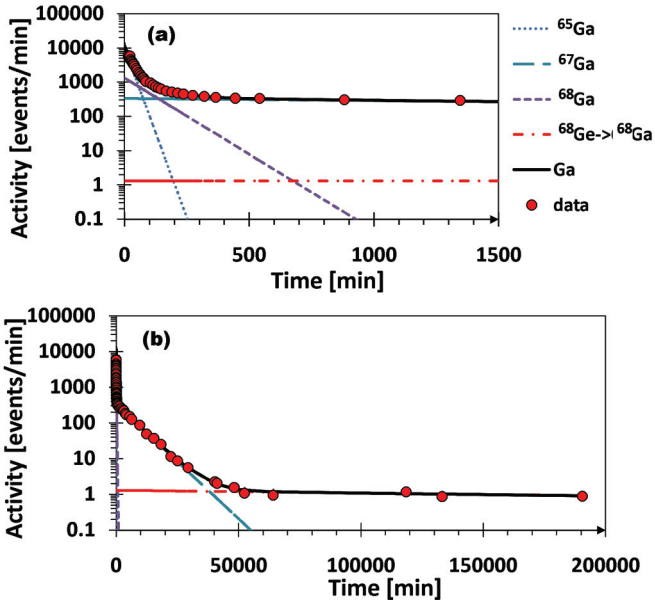

FIG. 5. (Color online) Activity curve for the Ga isotopes relative to the collision ^{6}Li + ^{64}Zn at 20 MeV. The bottom curve (b) is the same as the top one (a) but plotted on a longer time range. The time $t = 0$ corresponds to the end of the activation. The continuous line is the result of the fit procedure, whereas the other lines represent the contribution of individual nuclides to the total activity. The presence of a contribution having an apparent half-life of 270 d is attributable to the decay of ^{68}Ge ($T_{1/2} = 270$ d) into ^{68}Ga ($T_{1/2} = 67$ min).

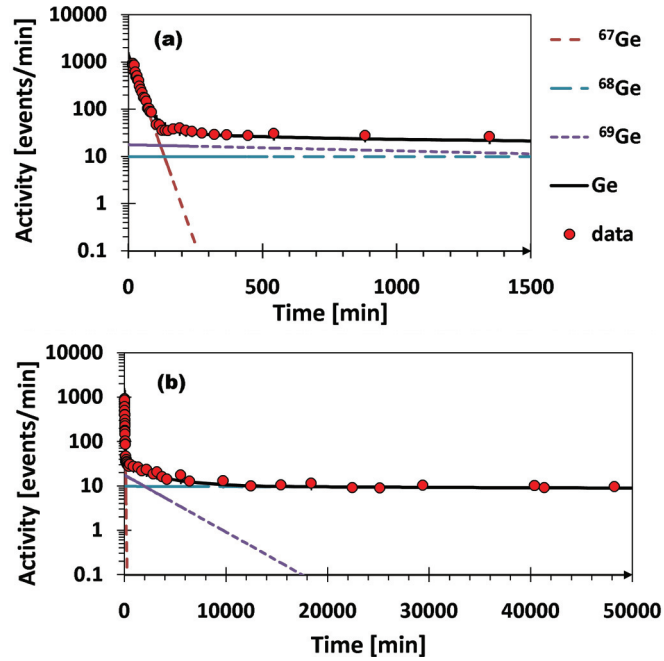

FIG. 6. (Color online) Same as Fig. 5 but for the Ge isotopes. Note that although plotted up to $t = 5 \times 10^4$ min, the activity was measured and fitted up to about $t = 2 \times 10^5$ min.

C. Reconstruction of the production cross sections

The determination of the production cross sections of the heavy fragments from the x-ray activity measurements requires knowledge of different parameters such as the activity of the considered isotope present in the target at the end of the activation, the K_α fluorescence probability, the total x-ray detection efficiency, the thickness of the activated targets, and the beam current as a function of time during the activation.

The first step in the extraction of the cross section is to convert the measured activity at the end of the activation $A(0)$ into the corresponding number of isotopes of the considered kind. To do that, the measured value has to be corrected for the x-ray detection efficiency determined as discussed in the previous section. Moreover, because the measured activity has been extracted by looking at the intensity of the K_α lines, one has to correct it also for the K_α fluorescence probability of the considered isotope. Such a fluorescence probability takes into account that the electron capture decay can be in competition with other decay modes and that the daughter atoms do not deexcite only by K_α emission, but also emit Auger electrons and x-rays corresponding to different transitions. The implantation profile of the different ERs inside the target + catcher has been calculated to correct for the emitted x-ray absorption in the target and catcher foils. Such calculations have been performed using a modified version of the MOCADIFUSION code [33], which, in turn, is based on the use of the the PACE [34] and SRIM [31] codes for the statistical model and energy loss calculations, respectively. Correction owing to x-ray absorption turned out to be on the order of 5%.

Once the number of atoms of a given isotope at the end of the activation is known, we have to extract the corresponding cross sections, taking into account that, during the activation, the population of a given isotope is competing with its decay. To do so, we used a numerical procedure. As previously discussed, we measured the number of incident beam particles as a function of time. Using this information and the known thickness of the irradiated foil, we divided the irradiation time into 10-s steps, and, assuming a unitary production cross section $\sigma = 1$ mb, we took into account formation and decay of the considered nuclide at each irradiation step. The ratio between the number of isotopes at the end of the activation and the one obtained assuming the unitary cross section gives the production cross section of the considered isotope. It is important to recall that some short-lived nuclides produced in the studied reactions, such as ^{65}Ga ($T_{1/2} = 15.2$ min) or ^{67}Ge ($T_{1/2} = 18.9$ min), decay into longer lived nuclides which are also directly produced in the collisions. The presence of such feeding processes has been properly taken into account when extracting the cross sections for the different residues.

III. RESULTS AND DISCUSSION

A. Excitation functions

To extract the TF cross section at each energy, we assumed that the HR production measured in this paper is attributable mainly to CF and ICF reactions. With this assumption, the TF cross section has been obtained, summing up the cross sections for the production of the different HRs at the considered energy. The experimental data have to be corrected to take into account the production of stable residues which cannot be detected with the used activation technique. To have an

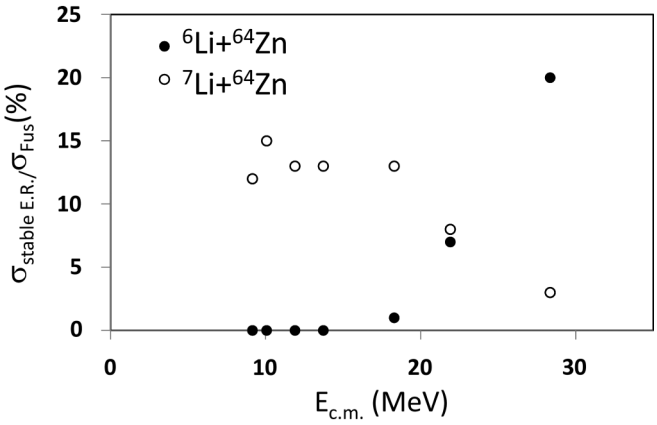

FIG. 7. Fraction of stable ER predicted by CF calculations performed with the code CASCADE as a function of the center-of-mass energy for the collisions ^{6}Li + ^{64}Zn (solid symbols) and ^{7}Li + ^{64}Zn (open symbols).

idea of this contribution, in Fig. 7 we show, for the present bombarding energies, the fraction of stable ER predicted by the code CASCADE [35] for CF, which was used to correct the measured cross sections. These calculations have been performed using standard input parameters either calculated internally or suggested in the code manual. It is important to notice that, as discussed in the next section, CF is the dominant mechanism at above-barrier energies, whereas capture of the deuteron (for ^{6}Li + ^{64}Zn) or of tritium (for ^{7}Li + ^{64}Zn) and single-nucleon transfer appear to be important at lower energies. In the region below the barrier, the fraction of stable ER in d capture is predicted to be close to zero as for CF; on the contrary, the fraction of stable ER in t capture is larger than the one for CF used to correct the data. Therefore, to take into account the possible effects of stable ER in t capture below the barrier, we asymmetrically increased by 10% the error bars in the excitation function for ^{7}Li + ^{64}Zn for $E_{c.m.} < 14$ MeV. The obtained TF excitation functions after this correction for the ^{6}Li + ^{64}Zn and ^{7}Li + ^{64}Zn systems are shown in Figs. 8

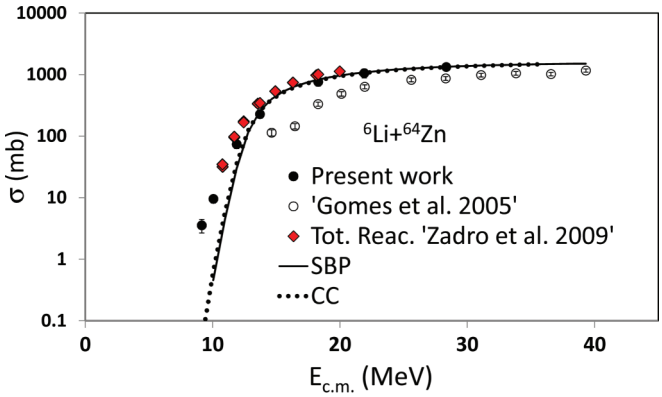

FIG. 8. (Color online) Present TF excitation function for ^{6}Li + ^{64}Zn (solid circles) compared with fusion data of Gomes *et al.* [19] (open circles) and total reaction data of Zadro *et al.* [12] (diamonds) for the same system. The continuous and dotted lines represent the results of single-barrier and CC calculations, respectively, for CF (see text for details).

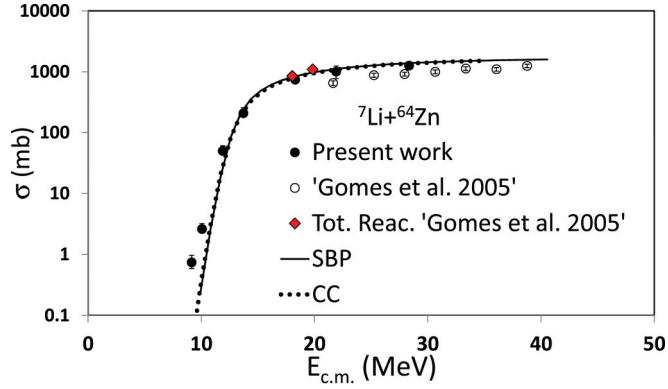

FIG. 9. (Color online) Present TF excitation function for ^{7}Li + ^{64}Zn (solid circles) compared with fusion data (open circles) and total reaction data (diamonds) of Gomes *et al.* [19] for the same system. The continuous and dotted lines represent the results of single-barrier and CC calculations, respectively, for CF (see text for details).

and 9. Horizontal error bars in these figures, related to the beam energy variation inside the Zn layer and calculated taking into account the target nonuniformity, are smaller than the symbols.

In Fig. 8, together with the present ^{6}Li + ^{64}Zn fusion data, we also show the TF excitation function for the same system from Ref. [19] and our total reaction excitation function from Ref. [12]. As one can see, the present TF cross sections appear to be systematically larger than the ones of Ref. [19], especially in the lower energy region. In Fig. 9 the present fusion data for ^{7}Li + ^{64}Zn are compared with the TF and total reaction cross sections for the same system presented in Ref. [19]. The comparisons shown in Figs. 8 and 9 appear to confirm the presence of an underestimation of the ^{6,7}Li + ^{64}Zn fusion cross sections of Ref. [19], as suggested by some of the authors of Ref. [19] in Ref. [26]. The fusion cross sections of Ref. [19] have been extracted detecting directly the emitted HRs and integrating their yield, and a possible reason for the observed underestimation could be related to the energy threshold in the direct HRs detection. On the contrary, the activation technique used in the present study is not affected by such kind of problems.

The continuous lines in Figs. 8 and 9, represent the CF excitation functions calculated within the single-barrier penetration (SBP) model, obtained by using a bare potential. The bare potential consisted of a double-folding real part and a Woods-Saxon imaginary part with parameters $W = 50$ MeV, $R_W = 1.0 \times (A_P^{1/3} + A_T^{1/3})$ fm, $a_W = 0.3$ fm [2], where A_P and A_T are the masses of the projectile and target, respectively. The very short-range imaginary potential accounts for fusion absorption of the flux that penetrates the Coulomb barrier [36]. The Coulomb potential of a uniformly charged sphere of radius $R_C = 1.25 \times (A_P^{1/3} + A_T^{1/3})$ fm was used in the calculations. The double-folding potential was calculated using the M3Y effective interaction in the form given in Ref. [37]. The matter densities for ^{6}Li and ^{64}Zn were obtained from the charge distributions for these nuclei taken from Refs. [38–40], respectively. The matter density for ^{7}Li was taken from Ref. [41]. The double-folding potential was calculated with the code DFPOT [42] and the fusion cross sections were calculated using the code FRESCO [43]. The TF experimental data

above the barrier are well reproduced by the one-dimensional barrier calculations, whereas, below the barrier, one has an enhancement with respect to the single-barrier calculations. To understand whether the observed enhancement could be explained by coupling effects to excited states of target or projectiles, we also performed coupled-channels (CC) calculations. Such calculations included two low-lying target states, the 2^+ state at 0.992 MeV and the 3^- state at 2.998 MeV. For the ^{6}Li projectile, we included the 3^+ and 2^+ unbound resonant states at 2.186 and 4.312 MeV, respectively. For the ^{7}Li projectile the first excited state $1/2^-$ at 0.478 MeV and the resonant state $7/2^-$ at 4.652 MeV were taken into account. The results of these calculations are shown as dotted lines in Figs. 8 and 9. Further details on these calculations can be found in Ref. [44]. The maximum enhancement of the CC predictions with respect to the SBP calculation, of the order of 40%, is observed at the lowest measured energies and is hardly visible in the figures. As one can see, the CC calculations do not reproduce the experimental data. Therefore, the low-energy enhancement of the experimental data with respect to the SBP calculations has to be attributable to coupling effects to other channels and/or to the presence of reaction mechanisms different from CF, as discussed in the next section.

As mentioned in the Introduction, the ratio of the ^{6}Li- to ^{7}Li-induced TF excitation functions with different targets shows an increasing trend below the barrier (see, e.g., Refs. [22–24,27]). The origin of this behavior was studied in Refs. [23,27] for the systems ^{6,7}Li + ^{59}Co within the CDCC frame. It was concluded that, at least for the ^{6,7}Li + ^{59}Co systems, such behavior is attributable to the different breakup thresholds of ^{6,7}Li. As shown in Fig. 10, the present ratio between the ^{6}Li- and ^{7}Li-induced TF cross sections is in agreement with this systematic trend. The old experimental data and related Coulomb barrier values V_b, used in Fig. 10, were taken from Ref. [22], whereas the Coulomb barrier value used to reduce the present ^{6,7}Li + ^{64}Zn data was 13.1 MeV. Although we did not perform dedicated calculations to reproduce the observed cross-section ratio, it is important to underline that, as discussed in the next section, in the low-energy region one has a dominant contribution of processes different than CF such as ICF or direct cluster transfer and single nucleon transfer. Therefore, a different yield for such processes in the two systems could contribute to the observed enhancement effect in the ^{6}Li case.

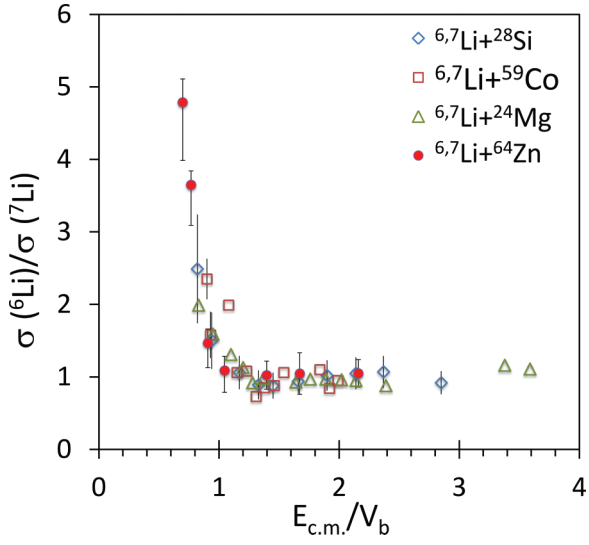

FIG. 10. (Color online) Ratio of the ^{6}Li- to ^{7}Li-induced TF excitation functions as a function of the reduced center-of-mass energy for the present data (solid red symbols), compared with same ratio on different targets taken from [22]) (open symbols). See text for details.

B. Comparison with statistical model calculations and reaction mechanisms

Results of the previous section already suggest that reaction mechanisms different than CF might become important at energies below the barrier. As underlined before, ^{6}Li and ^{7}Li have pronounced α-d and α-t cluster structures, with corresponding separation energies $S_\alpha = 1.47$ MeV and $S_\alpha = 2.47$ MeV, respectively. Therefore, we can expect, for instance, reactions where only an α particle or a d (in the ^{6}Li case) or a t (in the ^{7}Li case) are captured by the target. This may happen in two different ways. One possibility is to have a two-step process: breakup of the projectile followed by fusion of one of the two projectile fragments with the target, a process that is usually called ICF or breakup fusion (see, e.g., Refs. [1,45,46]). Another possibility is to have a single-step process, i.e., a direct cluster transfer (DCT), sometimes also called in the literature massive transfer, e.g., Ref. [45]. The competition between these two modes in collisions involving ^{6,7}Li has been mentioned in different papers (see, e.g., Refs. [15,22,45–47]). In collisions on heavy targets it has been suggested that the two-step ICF is the dominant capture mechanism of α, d, and t projectile clusters by the target, e.g., Refs. [15,45,46]. In some experiments with lower mass targets such as ^{59}Co or ^{28}Si, in spite of the lower Coulomb field, it was also suggested that the two-step ICF could be more likely than a DCT, although the authors specify that the observed hints are not conclusive and that one may have a coexistence of the two modes [22,47]. In the case of the present study, because we are using an activation technique, information on reaction mechanisms populating the observed HRs can be obtained only from the experimental relative yield of the different residues. As a consequence, as we will discuss in the following, a one-step DCT of a d, a t, or an α particle cannot be distinguished from a two-step ICF process of the same clusters. Indeed, excitation energies of nuclei formed in a two-step ICF process of a projectile cluster can be estimated as $E^* = (E_{\text{c.m.}} - S_\alpha) \times m_{\text{clu}}/m_p + Q_{\text{clu-}^{64}\text{Zn}}$, where $E_{\text{c.m.}}$ is the center-of-mass energy of the colliding system, S_α the α separation energy, m_{clu} and m_p the mass of the captured cluster and of the projectile, respectively, and $Q_{\text{clu-}^{64}\text{Zn}}$ the Q value for the fusion of the considered cluster with the target. Excitation energies of the same nuclei formed in a DCT can be estimated as $E^* = Q_{\text{gg}} - Q_{\text{opt}}$, where Q_{gg} is the ground-state Q value for the considered process and Q_{opt} is the optimum Q value given classically by trajectory-matching considerations. Here the following approximation has been used: $Q_{\text{opt}} = (Z_3Z_4/Z_1Z_2 - 1) \times E_{\text{c.m.}}$, where the subscripts 1,2 and 3,4 refer to the entrance and exit channels and $E_{\text{c.m.}}$

TABLE I. Estimated excitation energies for ICF or DCT of a projectile cluster in ^{6}Li + ^{64}Zn, for three selected bombarding energies. All the energies are expressed in MeV.

$E_{c.m.}$	E^* d-ICF	E^* d-DCT	E^* α-ICF	E^* α-DCT
28.3	19.8	18.2	21.3	20.2
13.7	14.9	13.6	11.5	10.8
10.1	13.7	12.5	9.1	8.4

is the center-of-mass energy in the entrance channel. For a given cluster capture, the estimated excitation energies for the two-step ICF and DCT are very similar, as one can see in Tables I and II for some selected bombarding energies.

For all d, t, and α cluster captures we performed CASCADE calculations for the decay of the formed nuclei assuming the excitation energies estimated for the two mechanisms, finding, as expected, similar relative yield of the residues for ICF and DCT. Therefore, there is no way to distinguish between the two contributions with the present experimental technique. For this reason, to be exact, from now on, we refer to the projectile cluster capture process as ICF/DCT. CASCADE calculations for ICF/DCT were performed, as in the CF case, using default input parameters either internally calculated or suggested in the code manual and the excitation energies reported in Tables I and II. As discussed in the Introduction, in fusion reactions induced by ^{6,7}Li on medium mass or light targets, the simple identification of the residues is not sufficient to clearly separate CF from ICF/DCT contributions, because the same residue can be produced by both reaction channels. Nevertheless, a comparison of the measured relative yield of the residues, with the corresponding predictions of statistical model calculations, can give an idea of the relative importance of the CF and ICF/DCT channels.

In Fig. 11 we compare the experimental relative yields of the HRs with the predictions of statistical model calculations, obtained by using the code CASCADE [35], for the collision ^{6}Li + ^{64}Zn with standard (i.e., internally calculated or suggested in the manual) input parameters. Together with the relative yield expected for CF, we also show the predictions for the HR relative yield in the ICF/DCT of a d or of an α particle. To be exact, we specify that CASCADE ICF/DCT calculations shown in the figure have been performed assuming the ICF excitation energies quoted in Table I; as already mentioned, analogous calculations using the DCT excitation energies of Table I give similar relative yields. Although a detailed comparison between our data and the calculations cannot be done, because we do not experimentally separate the CF and ICF/DCT contributions, the comparison of Fig. 11 gives us some interesting information.

TABLE II. Estimated excitation energies for ICF or DCT of a projectile cluster in ^{7}Li + ^{64}Zn, for three selected bombarding energies. All the energies are expressed in MeV.

$E_{c.m.}$	E^* d-ICF	E^* d-DCT	E^* α-ICF	E^* α-DCT
28.3	26.9	22.2	18.2	19.2
13.7	20.6	17.6	9.8	9.8
10.1	19.1	16.5	7.8	7.4

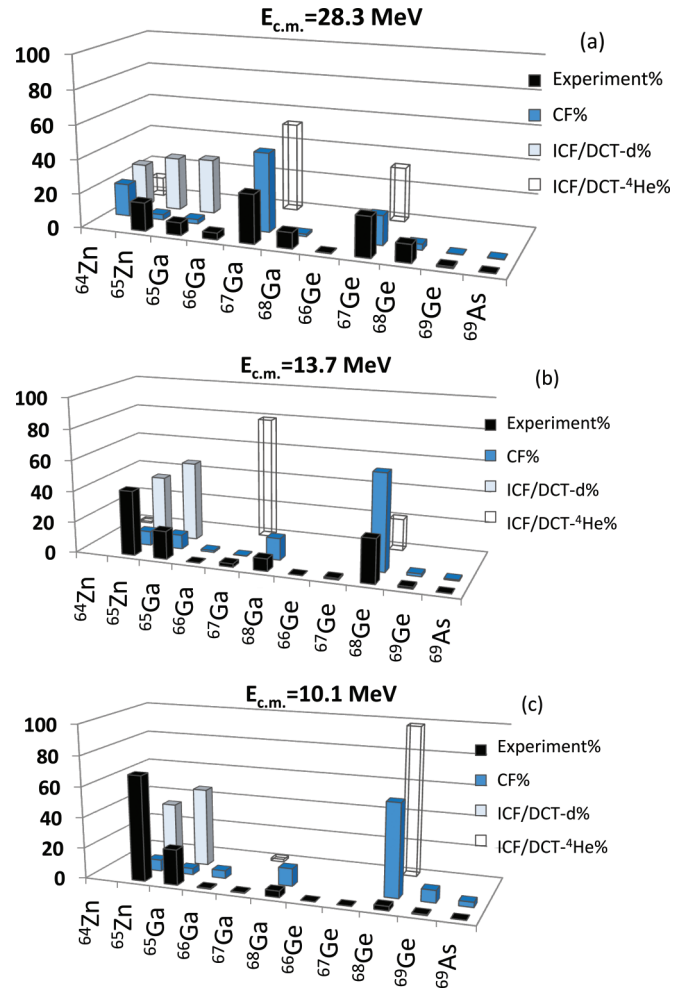

FIG. 11. (Color online) Experimental HR relative yield for ^{6}Li + ^{64}Zn (black bars) compared with the predictions of statistical model calculations for CF (blue bars), d-ICF/DCT (gray bars), and α-ICF/DCT (open bars) at different bombarding energies. Relative errors on the experimental data, not reported, are lower than 5% for the most populated residues. See text for details.

At energies well above the Coulomb barrier ($V_b \approx 13$ MeV [12]), the experimental relative yield is in reasonable agreement with the predictions for CF. Therefore, in this energy range, such process appears to be the dominant one, although the experimental extra yield observed for ^{65}Zn and ^{65}Ga, with respect to the CF calculations, could already indicate the presence of some deuteron ICF/DCT. As one can see in Fig. 11, CF calculations predict that the lower the bombarding energy, the larger becomes the yield for the heavier residues, owing to the lower amount of excitation energy available to evaporate particles. However, the experimental data show exactly the opposite trend, populating lighter residues for decreasing bombarding energies. As one can see, around the lowest measured energies the HR production is dominated by those residues (^{65}Zn and ^{65}Ga) which are expected in d-ICF/DCT. Such a behavior clearly shows that the lower the bombarding energy, the more important are processes different than CF like the d-ICF/DCT. For the similar ^{6}Li + ^{59}Co system, an important yield for d-ICF was inferred from the comparison between statical

model calculations and the experimental residue cross sections [23], as well as from the measurements of light particle spectra [47]. It is also important to notice that, together with d-ICF/DCT, ^{65}Zn could also be populated by $1n$-transfer reactions having $Q_{gg} = +2.3$ MeV, whereas ^{65}Ga could be also populated by a $1p$ transfer ($Q_{gg} = -0.49$ MeV). Actually, in, e.g., Refs. [48–50] it is shown that in ^{6}Li- and ^{7}Li-induced collisions breakup triggered by nucleon transfer is an important channel.

To check the possible relevance of transfer channels, we calculated the cross sections for the stripping of $1n$ and $1p$ in the case of both the reactions under investigation. Finite-range distorted-wave Born approximation (DWBA) calculations were performed using the code FRESCO [43]. For the projectile, only the ground-state overlaps were considered, whereas, for the target-like, the overlaps between the ground state and several excited states, up to 1 MeV excitation energy in the case of $1n$ transfer and 3 MeV in the 1-p transfer case, were considered. The states included were the ones for which spectroscopic amplitudes were known in the literature taking into account that, for Q-matching considerations, low excitation energies are expected. The spectroscopic amplitudes were taken from Refs. [51–53]. The calculations show that in the ^{6}Li + ^{64}Zn case, the experimentally measured ^{65}Ga and ^{65}Zn cross sections at the lowest energies are of the same order of the DWBA estimates, whereas above the barrier the experimental cross sections are larger than the DWBA estimated values.

In summary, because d-ICF/DCT and single-nucleon transfer cannot be clearly separated experimentally, and considering the results of the FRESCO calculations, the present data could also be affected by a non-negligible yield for single nucleon transfer below the barrier.

A comparison equivalent to the one of Fig. 11, is shown in Fig. 12 for the ^{7}Li + ^{64}Zn system. Analogously to Fig. 11 the CASCADE ICF/DCT calculations have been performed assuming the ICF excitation energies of Table II, but similar relative yields would have been obtained using the DCT excitation energies of the same table. Such a comparison shows a behavior similar to the one observed for ^{6}Li + ^{64}Zn, with CF predictions reasonably reproducing the experimental data well above the barrier. Once more, contrary to the prediction of CASCADE CF calculations, the experimental data populate lighter residues for decreasing bombarding energies. Around the lowest measured energies the HR production is once more dominated by those residues (^{65}Zn and ^{66}Ga) which are expected in t-ICF/DCT and $1n$ transfer. Indeed, clear experimental evidence of $1n$ transfer reactions from the projectile to the target for the present colliding system is shown in Ref. [44]. In addition, the previously mentioned DWBA calculations performed with FRESCO predicts cross sections for this processes on the order of the measured cross sections at the lowest energies. The DWBA cross section for the $1p$ transfer producing ^{65}Ga is consistent with zero, as experimentally measured, owing to the high negative Q_{gg}. The single-nucleon transfer process cannot explain the production of ^{66}Ga experimentally observed in the reaction with the ^{7}Li beam at low energy, which could be attributable to an ICF/DCT contribution.

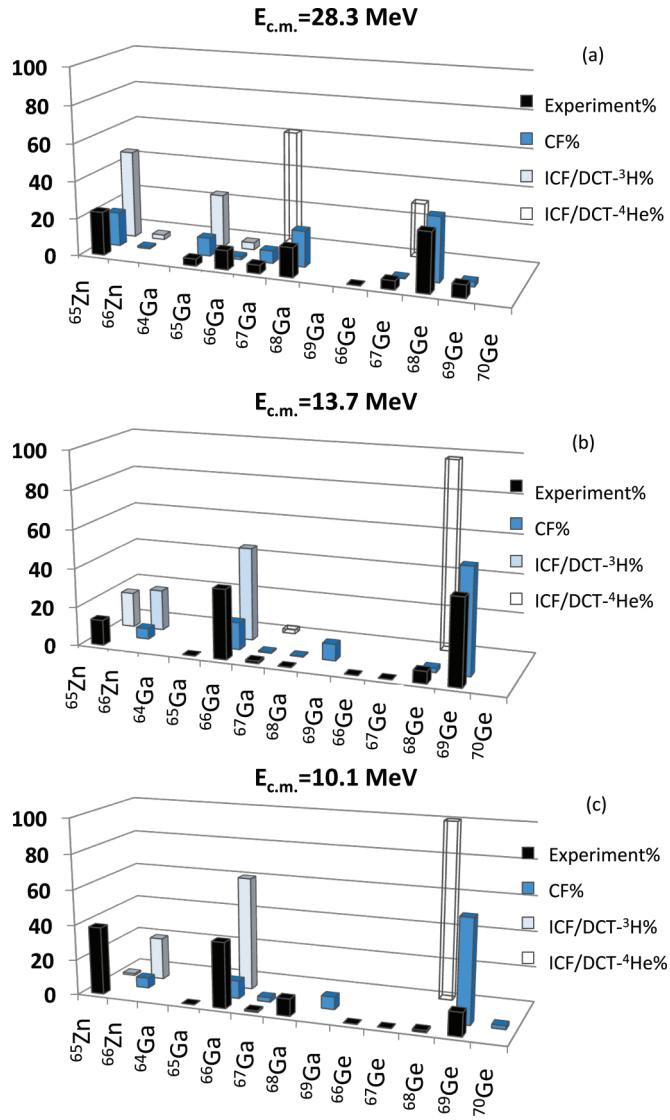

FIG. 12. (Color online) Experimental HR relative yield for ^{7}Li + ^{64}Zn (black bars) compared with the predictions of statistical model calculations for CF (blue bars), t-ICF/DCT (gray bars), and α-ICF/DCT (open bars) at different bombarding energies. Relative errors on the experimental data, not reported, are lower than 5% on the most populated residues. See text for details.

An attempt was also made to perform the DCT calculations with FRESCO within the cluster model both for ^{6}Li- and ^{7}Li-induced collisions, but in a very approximate way because the spectroscopic amplitudes are not known. Contrary to the single-nucleon transfer case, owing to Q-matching considerations, high excitation energies are expected, as shown in Tables I and II. These calculations predict negligible cross-sections for d transfer and t transfer in the case of the ^{6}Li and ^{7}Li beam, respectively.

In summary, the comparison of the experimental data with SBP calculations and statistical model predictions clearly shows that CF is the dominant process at above-barrier energies, whereas below the barrier different processes such as d-ICF/DCT (for ^{6}Li + ^{64}Zn), t-ICF/DCT (for ^{7}Li + ^{64}Zn), and single-nucleon transfer are dominating.

IV. SUMMARY AND CONCLUSIONS

We measured the HR excitation functions for the ^{6,7}Li + ^{64}Zn systems around the Coulomb barrier. To avoid energy threshold problems linked to the direct detection of the slow HRs, their production cross sections were measured by using an activation technique, detecting off-line the atomic x-rays emitted after the electron capture decay of the residues. Our experimental cross sections are larger than the ones reported in Ref. [19] for the same systems, especially in the lower energy region. This result appears to confirm the possible underestimation of the ^{6,7}Li + ^{64}Zn fusion data of Ref. [19], as suggested by some of the authors of Ref. [19] in Ref. [26].

The HR excitation function ratio between the ^{6}Li- and ^{7}Li-induced collisions shows an increasing trend as the energy decreases below the barrier, as observed by other authors [22–24] for similar systems.

The experimental relative yields of the HRs have been compared with the predictions of the statistical model code CASCADE [35]. Such a comparison suggests that HR production is dominated by CF at above-barrier energies, whereas different processes, like ICF/DCT or even single-nucleon transfer, become dominant in the sub-barrier energy region. In summary, the study of fusion reactions induced by light weakly bound nuclei on medium mass targets presents a number of experimental challenges. Although the experimental problems related to the low energy of the produced HR can be overcome by using activation or on-line γ-ray techniques, a clear separation of CF from ICF, DCT, or even single-nucleon transfer processes in the experimental data cannot be easily achieved and transfer might actually contaminate what are believed to be TF excitation functions. Therefore, new experiments able to clearly separate the contribution of different reaction mechanisms in the HR production are needed for a better understanding of fusion in collisions induced by light weakly bound projectiles around the Coulomb barrier.

ACKNOWLEDGMENTS

The authors would like to thank Professor P. R. S. Gomes for several stimulating discussions and Professor A. M. Moro for his help with the FRESCO calculations.

[1] L. F. Canto *et al.*, Phys. Rep. **424**, 1 (2006).
[2] N. Keeley *et al.*, Prog. Part. Nucl. Phys. **59**, 579 (2007).
[3] N. Keeley *et al.*, Prog. Part. Nucl. Phys. **63**, 396 (2009).
[4] A. Vitturi, Eur. Phys. J. Spec. Top. **156**, 237 (2008).
[5] A. Di Pietro *et al.*, Phys. Rev. Lett. **105**, 022701 (2010).
[6] A. Di Pietro *et al.*, Phys. Rev. C **85**, 054607 (2012).
[7] Y. Sakuragi, Phys. Rev. C **35**, 2161 (1987).
[8] N. Keeley *et al.*, Nucl. Phys. A **571**, 326 (1994).
[9] A. M. M. Maciel *et al.*, Phys. Rev. C **59**, 2103 (1999).
[10] A. Pakou *et al.*, Phys. Rev. C **69**, 054602 (2004).
[11] H. Kumawat *et al.*, Phys. Rev. C **78**, 044617 (2008).
[12] M. Zadro *et al.*, Phys. Rev. C **80**, 064610 (2009).
[13] J. M. Figueira *et al.*, Phys. Rev. C **81**, 024613 (2010).
[14] N. N. Deshmukh *et al.*, Phys. Rev. C **83**, 024607 (2011).
[15] M. Dasgupta *et al.*, Phys. Rev. C **70**, 024606 (2004).
[16] P. R. S. Gomes *et al.*, Phys. Rev. C **73**, 064606 (2006).
[17] Y. W. Wu *et al.*, Phys. Rev. C **68**, 044605 (2003).
[18] M. K. Pradhan *et al.*, Phys. Rev. C **83**, 064606 (2011).
[19] P. R. S. Gomes *et al.*, Phys. Rev. C **71**, 034608 (2005).
[20] R. M. Anjos *et al.*, Phys. Lett. B **534**, 45 (2002).
[21] G. V. Marti *et al.*, Phys. Rev. C **71**, 027602 (2005).
[22] M. Sinha *et al.*, Eur. Phys. J. A **44**, 403 (2010).
[23] C. Beck *et al.*, Phys. Rev. C **67**, 054602 (2003).
[24] M. Ray *et al.*, Phys. Rev. C **78**, 064617 (2008).
[25] L. F. Canto *et al.*, Nucl. Phys. A **821**, 51 (2009).
[26] P. R. S. Gomes, J. Lubian, and L. F. Canto, Phys Rev. C **79**, 027606 (2009).
[27] A. Diaz-Torres, I. J. Thompson, and C. Beck, Phys. Rev. C **68**, 044607 (2003).
[28] A. Di Pietro *et al.*, Phys. Rev. C **69**, 044613 (2004).
[29] V. Scuderi *et al.*, Phys. Rev. C **84**, 064604 (2011).
[30] A. Di Pietro, Eur. Phys. J. Spec. Top. **150**, 15 (2007).
[31] J. F. Ziegler, www.srim.org.
[32] National Nuclear Data Center, www.nndc.bnl.gov.
[33] M. Mazzocco *et al.*, Nucl. Instrum. Methods B **266**, 3467 (2008).
[34] A. Gavron, Phys. Rev. C **21**, 230 (1980).
[35] F. Puhlhofer, Nucl. Phys. A **280**, 267 (1977).
[36] M. J. Rhoades-Brown and P. Braun-Munzinger, Phys. Lett. B **136**, 19 (1984).
[37] G. R. Satchler and W. G. Love, Phys. Rep. **55**, 183 (1979).
[38] G. C. Li, I. Sick, R. R. Witney, and M. R. Yearian, Nucl. Phys. A **162**, 583 (1971).
[39] R. Neuhausen, J. J. W. Lightbody, S. P. Fivozinsky, and S. Penner, Phys. Rev. C **5**, 124 (1972).
[40] C. W. De Jager, H. De Vries, and C. De Vries, At. Data Nucl. Data Tables **14**, 479 (1974).
[41] J. Cook, M. F. Vineyard, K. W. Kemper, and V. Hnizdo, Phys. Rev. C **27**, 1536 (1983).
[42] J. Cook, Comput. Phys. Commun. **25**, 125 (1982).
[43] I. J. Thompson, Comput. Phys. Rep. **7**, 167 (1988).
[44] M. Zadro *et al.*, Phys. Rev. C **87**, 054606 (2013).
[45] A. Shrivastava *et al.*, Phys. Lett. B **718**, 931 (2013).
[46] V. Tripathi *et al.*, Phys. Rev. C **72**, 017601 (2005).
[47] F. A. Souza *et al.*, Nucl. Phys. A **821**, 36 (2009).
[48] D. Luong *et al.*, Phys. Lett. B **695**, 105 (2011).
[49] D. Luong *et al.*, Eur. Phys. J. Web Conf. **17**, 03002 (2011).
[50] A. Shrivastava *et al.*, Phys. Lett. B **633**, 463 (2006).
[51] S. Cohen and D. Kurath, Nucl. Phys. A **101**, 1 (1967).
[52] J. V. Hienen, W. Chung, and B. Wildenthal, Nucl. Phys. A **269**, 159 (1976).
[53] M. Betigeri, H. Duhm, R. Santo, R. Stock, and R. Bock, Nucl. Phys. A **100**, 416 (1967).